Turbulence Manipulation to Increase Effective Reynolds Numbers in Vehicle Aerodynamics

J. Wiedemann*
AUDI AG, Ingolstadt, Federal Republic of Germany
and
B. Ewald†
Technical University of Darmstadt, Darmstadt, Federal Republic of Germany

In the testing of small-scale models of road vehicles Reynolds number requirements usually are violated. Instead of increasing the freestream velocity (Mach number problems), the approach in the present paper makes use of Taylor's theory on the interdependence between the intensity and structure of freestream turbulence and the Reynolds number corresponding to a defined location of the point of transition. Two differently scaled principle models of a passenger car were tested in the wind tunnel. Reynolds numbers (based on overall length) varied from 1.7×10^6 to 5.2×10^6. The resulting drag coefficients (c_D) decreased from 0.40 to 0.28, and the overall flow structure changed significantly, which can be seen from the pressure distributions. When a screen of adequate mesh and bar size in the nozzle outlet is used, pressure distributions corresponding to different Reynolds numbers nearly fall onto a single curve that is equivalent to an increase of the effective Reynolds number. Analogous to the critical Reynolds number of the sphere, a Reynolds number corresponding to a fixed value of c_D can be defined.

Nomenclature

A = constant, Eqs. (2) and (8)
c_D = drag coefficient
c_p = pressure coefficient
d = rod diameter of turbulence screen
D = sphere diameter
L = macroscale of turbulence
M = mesh size of turbulence screen
p = pressure
Tu = turbulence intensity for isotropic turbulence
Tu_x = intensity based on u' for real turbulence ($Tu_x = u'/U_\infty$)
u = longitudinal component of velocity
U = inviscid flow velocity along a body contour
U_∞ = freestream velocity
x = streamwise coordinate, Fig. 3
λ = dissipative eddy scale, Eq. (1)
Λ = pressure gradient parameter, Eq. (4)
ν = fluid kinematic viscosity
ρ = fluid density

Subscripts and Superscripts

tr = transition
1 = refers to screen 1
2 = refers to screen 2
$'$ = fluctuating quantity

Introduction

In contrast to most other aeronautical problems, road vehicle aerodynamics can be investigated either by full- or small-scale experiments. Usually, full-scale wind-tunnel testing is very costly because it requires large wind tunnels and expensive models. During the early design-definition stages, a lot of shape modifications have to be modeled and tested. With full-scale clay models, this is a time-consuming procedure that leads to a very inefficient use of the wind-tunnel facility. Most of the early work also can be done by using small-scale models. Typical scales are 1:5 to 1:2.5. When scaling down cars, one has to find a good compromise between weight and transport requirements, demands of model wind tunnels, manufacturing accuracy of the model, and full-scale flow simulation (Reynolds number effects). Quarter-scale models offer very considerable savings in volume and mass (1/64) and test section area (1/16), the latter being very important if tests have to be performed with smaller than full-scale blockage ratio, which is mostly of the order of 5–10%.

Generally, Reynolds number deviations are not too large. A full-scale test of a car with a total length of $L_M = 4$ m at a freestream velocity of 140 km/h in air represents a Reynolds number of about $Re = 1 \times 10^7$. Good model tunnels allow for experiments at $U_\infty = 210$ km/h. In this way, a Reynolds number of 3.9×10^6 can be achieved, which is already more than 1/3 of the full-scale value. In addition, most of today's car shapes are not very sensitive to Re effects. Typical errors in predictions of drag coefficients with quarter-scale saloon cars are of the order of 2%. Nevertheless, there are vehicle configurations that reveal considerably greater sensitivity to Reynolds number deviations. In general, this is due to radii on the contour (R = 40–120 mm, full-scale), where the flow undergoes transition when changing from a quarter- to a full-scale model for constant freestream velocity of the order of 140 km/h. The potential for increasing U_∞. for the small-scale model might be limited due to Mach number effects. They become important even for rather low values of the freestream Mach number if there are regions of very low pressure (the radii!) along the contour.

There are several ways of increasing the quality of scale model wind-tunnel testing:

1) The cooling system can be simulated by a so-called universal radiator simulator, which, without correctly representing the geometrical details of internal flow ducts, ensures the correct volume flow and interaction with the exterior flow.

Received March 24, 1988; presented as Paper 88-2028 at the AIAA 15th Aerodynamic Testing Conference, San Diego, CA, May 18–20, 1988; revision received July 8, 1988.

*Doctor of Mechanical Engineering, Aerodynamics.
†Professor of Mechanical Engineering, Aerodynamics and Measuring Techniques. Member AIAA.

2) Advanced ground simulation by tangential blowing, distributed suction, or moving belt technique can be used.

3) Turbulence manipulation can be used to decrease *Re* effect.

In this paper, only the method of turbulence manipulation will be discussed. For more information on points 1 and 2, see the papers by Wiedemann[1,2] and Soja and Wiedemann.[3] Many wind-tunnel engineers in the aircraft industry successfully make use of tripping wires to locate transition lines on wings and fuselages. With cars, usually little is known about transition. Moreover, tripping wires complicate the work on clay models with Reynolds-sensitive shapes. For a complex configuration like a road vehicle, it seems to be more comfortable and effective to manipulate the turbulence of the oncoming flow.

From Taylor's theory,[4,5] which is briefly reviewed in the next section, it is known that there exists a correlation between the Reynolds number of transition Re_{xtr} and the turbulence intensity and scale of the oncoming flow. So, for bodies whose drag is due mainly to Reynolds number–dependent flow separation, e.g. the sphere, there is a possibility of simulating higher Reynolds numbers by just increasing the freestream turbulence intensity, provided its scale is adjusted to the flow problem of interest. For the sphere, Dryden et al.[6] proved this by experiment. In the seventies and earlier there were some experiments, e.g., in the German aircraft industry, dealing with this concept. Though there were difficulties in matching the artificial turbulence to the flow problem of interest, tests turned out to be successful in increasing $c_{L\max}$. However, the c_D shift toward higher Reynolds numbers was not possible, because the drag of the wing is mainly due to friction but not to separation.

Taylor's Theoretical Considerations Concerning Transition and Separation and their Relation to Freestream Turbulence Intensity and Scale

The theoretical justification for turbulence manipulation by screens and grids is given by Taylor in his "Statistical Theory of Turbulence."[4,5] In contrast to Tollmien's analysis, Taylor came to the conclusion that for boundary-layer flow, "the Reynolds number corresponding with the change from steady to turbulent flow depends only on the turbulence of the stream...." That means that a boundary layer is affected by the action of local pressure gradients that accompany the oncoming turbulent flow. The mean magnitude of these fluctuating pressure gradients is connected with the scale of the smallest eddies (λ), which are responsible for the dissipation of energy in turbulent motion. For *isotropic* turbulence,

$$\sqrt{\overline{\left(\frac{\partial p'}{\partial x}\right)^2}} = 2\sqrt{2}\rho\,\frac{u'^2}{\lambda} \tag{1}$$

where u' is used as an abbreviation for the rms value of the u-component velocity fluctuation.

For turbulence produced in an airstream by passing through a rectangular grid of regular bars, the dissipative scale λ is related to M, the mesh size, by

$$\frac{\lambda}{M} = A\sqrt{\frac{\nu}{M \times u'}} \tag{2}$$

where A is a constant (see "Discussion of Results" section). From experiments it is known that Eq. (2) holds, provided $(u'M)/\nu$ is greater than about 60. This is the case for all the experiments discussed in this paper. Combining Eqs. (1) and (2) provides

$$\sqrt{\overline{\left(\frac{\partial p'}{\partial x}\right)^2}} = \frac{2\sqrt{2}}{A \times M}\rho u'^2\sqrt{\frac{u' \cdot M}{\nu}} \tag{3}$$

To arrive at a nondimensional form of the pressure gradient, Taylor introduced, for the case of boundary-layer flow, a pressure gradient parameter Λ' for the fluctuating pressure analogous to Λ, the well-known pressure gradient parameter for the steady motion in the Kármán-Pohlhausen theory. The rearrangement of Eq. (3) according to Λ' is given elsewhere.[4] A criterion for determining the location where the b. l. is turbulent is

$$\Lambda' = f_1\left(\frac{U \cdot x_{tr}}{\nu}\right) \tag{4}$$

As Taylor shows, this leads to

$$\left(\frac{u'}{U}\right) \cdot \left(\frac{x_{tr}}{M}\right)^{1/5} = f_2\left(\frac{U \cdot x_{tr}}{\nu}\right) = f_2(Re_{tr}) \tag{5}$$

Equation (5) gives a relation between the intensity (u'/U) and scale (M/x_{tr}) of isotropic turbulence and the Reynolds number (Re_{tr}) based on the distance from the leading edge to the location of transition (x_{tr}). Taylor showed that Eq. (5) also holds for the case of a sphere if U is replaced by U_∞ and x_{tr} by the sphere diameter D:

$$\left(\frac{u'}{U_\infty}\right) \cdot \left(\frac{D}{M}\right)^{1/5} = F\left(\frac{U_\infty \cdot D}{\nu}\right) = F(Re_{\text{crit}}) \tag{6}$$

In other words, replacing the variable x_{tr} by the constant diameter D introduces an arbitrary but constant angular position of transition. This, however, leads to a specific drag coefficient, the critical drag coefficient, at the critical Reynolds number Re_{crit}. Equation (6) was verified by the extensive experimental work of Dryden et al.[6] as shown in Fig. 1.

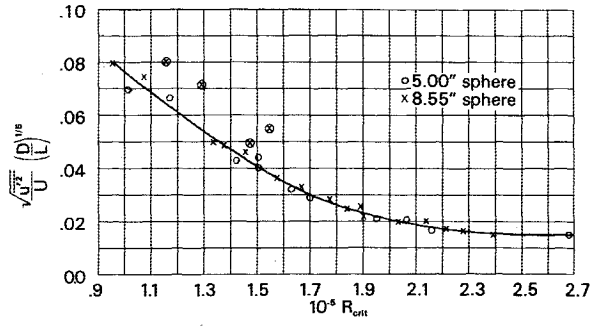

Fig. 1 Critical Reynolds number of a sphere vs $(u'/U_\infty) \times (D/L)^{1/5}$ as measured by Dryden et al.[6]

All the data from different screens and sphere diameters, except for the measurements made at a distance of 1 ft, lie remarkably well on a single curve within the observational errors. To account for the streamwise inhomogeneity of the grid turbulence, Dryden used L (actual macroscale) instead of M as a measure of the eddy size. This curve is the function F in Eq. (6), which *cannot* be obtained explicitly from Taylor's analysis. One of the goals of this paper is to show whether there are analogous functions for road vehicle configurations that also reveal *Re*-dependent drag coefficients due to changes in the location of transition and separation.

Experimental Setup

Wind Tunnel

All the experiments discussed in the next sections were carried out for Audi in the 3-m open-jet closed-circuit wind tunnel of the Institute for Aerodynamics and Measurement Techniques at the Technical University of Darmstadt, Federal Republic of Germany. In a pre-experiment, the flow quality in the test section was checked. Within the area covered by the cross section of the 1:2.5 model, which extended from $y = \pm 320$ mm in the lateral and $z = \pm 240$ mm in the vertical direction from the test section c. l., the dynamic pressure variations were found to be smaller than $\pm 0.5\%$ (peak to peak). Measurements were performed with a Prandtl probe.

The turbulence intensity on the c. 1. varied from $Tu_x = (u'/U_\infty) = 0.8\%$ at a distance of $x_1 = 0.1$ m behind the nozzle to 0.7% at $x_2 = 1.0$ m. The variations of Tu_x in the lateral and vertical directions were, based on c. 1. values, of the order of $-0.01\% \le \Delta Tu_x \le +0.03\%$ and $0\% \le \Delta Tu_x \le +0.02\%$, respectively.

Equipment for Turbulence Measurements

The turbulence measurements were performed with DISA CTA equipment, including the 56N SAE system and a 56 P 11 type wire. The length scales of the turbulent motion in the test section were obtained from the autocorrelation function, which results from a Fast Fourier transformation of the spectrum. Integration yields the time scale T, which is related to the macrolength scale L by

$$L = U_\infty \cdot T \tag{7}$$

The Taylor microscale (dissipative scale) was obtained by means of a parabola fit to the autocorrelation function (see Taylor[5]). The spectrum itself was measured with a spectrum analyzer Hewlett-Packard Model 5420A Digital Signal Analyzer.

Generation of Freestream Turbulence

Tests were performed with two alternative biplane square mesh screens with round bars located in the nozzle outlet plane. Screen 1 had following dimensions: mesh size (M_1)/bar diameter (d_1) 12.5 mm/1.0 mm and open to total area ratio $\beta_1 = 0.85$. The corresponding data for screen 2 was $M_2/d_2 = 19.0$ mm/1.4 mm and $\beta_2 = 0.86$.

During the pre-experiments, the streamwise extension of the individual wakes of the single rods was investigated. It was found that at a distance of 0.38 m behind screen 2, which is $(x/M_2) = 20$ in nondimensional coordinates, there is still a variation of the dynamic pressure of $\pm 1.8\%$. This is consistent with Taylor's findings.[5] He showed that the angle of turbulent diffusion is constant: $\alpha = 2.35Tu(x = 0)$ for isotropic turbulence. With an initial value of $Tu_x(x = 0) = 1.0\%$ at the position of the screen, one finds that $\alpha = 1.35$ deg. Thus, mixing of the individual wakes can be expected at $(x/M) = 39.1$ for screen 1 and 39.4 for screen 2, respectively.

The variations of the turbulence intensity for the lateral ($y-$) direction at $x = 0.38$ m and $z = 0$ behind screen 2 ($x/M_2 = 20$) amounted to $\Delta Tu_x = \pm 0.2\%$, which was five times higher than for the flow without screen ($-0.01\% \le \Delta Tu_x \le +0.03\%$). At $x = 0.6$ m ($-32M_2$), which is still below the value of $39.4M_2$ suggested by Taylor, the variations decreased to $-0.01\% \le \Delta Tu_x \le +0.14\%$, which coincides better with the data for the flow without a screen. For screen 1, the homogeneity of the undisturbed flow is already achieved at $x = 0.6$ m ($x/M_1 = 48$—no data was taken for smaller x!). So the theoretical prediction, $(x/M_1) = 39.1$, seems to make sense in this case as well. Nevertheless, since some of the pressure and force measurements were performed at $(x/M_1) = 32$ and $(x/M_2) = 21$, at least behind screen 2, nearly isotropic turbulence cannot be guaranteed for all the results obtained.

Vehicle Models and Setup in Test Section

Two identical models (scale 1:4 and 1:2.5) of a single principle vehicle shape without wheels and any details were manufactured from polyurethane foam and epoxy wood. The model dimensions (quarter-scale) are shown in Fig. 2. Several model sections were equipped with pressure taps, which were scanned by a Scanivalve system with a Statham PM131TC differential pressure transducer.

The model design, especially the radii R_1 and R_7 (see Fig. 2), was chosen in order to reveal the Reynolds number dependence of the drag coefficient. The freestream velocity ranged from $U_\infty = 25$ m/s to 49 m/s, which led to Re (based on model length L_M) between 1.7×10^6 (quarter-scale, $L_M = 1.0$ m) and 5.2×10^6 (scale 1:2.5, $L_M = 1.6$ m). As Re based on R_7 varied

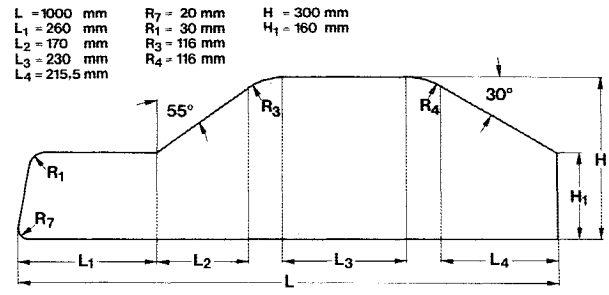

Fig. 2 Midsection of principle road vehicle shape for wind-tunnel tests. Measurements for quarter-scale model.

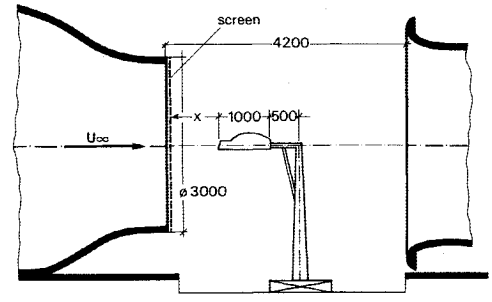

Fig. 3 Setup of road vehicle in the open test section.

from 3.3×10^4 (quarter-scale, $R_7 = 0.020$ m) to 1.0×10^5 (scale 1:2.5, $R_7 = 0.032$ m), a transition from laminar to turbulent flow could be expected.

The models were tested in the wind tunnel without ground plane. They were mounted on a sting equipped with an internal six-component strain gage balance. The blockage ratio of the models in the test section was small: 1.6% for the quarter scale and 4.2% for the 1:2.5 model. The experimental setup is sketched in Fig. 3. The model setup without ground board, though unrealistic for vehicle testing, was chosen in order to separate the effect of freestream turbulence on the vehicle from the effect on the boundary layer along the ground board.

According to the state-of-the-art in turbulent boundary-layer research, one can expect an impact on the boundary layer along a flat plate from freestream turbulence levels above 1% and macroscales on the order of characteristic boundary-layer scales. This leads to a fuller velocity profile, indicated by an increase of the relation of b. 1. thickness to momentum thickness. Furthermore, there is a decrease of the shape parameter and an increase of the wall shear stress coefficient, entrainment rate, and b. 1. thickness. See the work by Meier,[7] Meier and Kreplin,[8] Bradshaw,[9] Hancock,[10] and Hancock and Bradshaw.[11]

Some of these effects would be "favorable" in the sense that they may even serve to decrease the flow distortions that result from road vehicle tests over stationary ground boards, e.g., displacement of the freestream by the boundary layer. On the other hand, increased overall boundary-layer thickness is "unfavorable," especially when testing vehicles with very small ground clearance. Nevertheless, there is a strong tendency in vehicle aerodynamics to proceed, at least with scale models, toward advanced ground simulation by moving belt, tangential blowing, or distributed normal suction. Without rating the quality of each of these methods, one can say that they all decrease or nearly eliminate the distortions resulting from the boundary layer. Thus, small changes of the remaining boundary layer due to freestream turbulence are of very small significance to the overall flow.

Discussion of Results

Figure 4 displays the results of the freestream measurements of the turbulence intensity on the test section c. 1. vs the distance from the screen in the nozzle exit. It can be seen for

both screens that there is a region of x/M where the decay of turbulence follows a linear law. This is in agreement with Taylor's theoretical considerations.[5] He showed that there is a law of the form

$$\frac{U_\infty}{u'} = \frac{5}{A^2}\frac{x}{M} + \text{const} \tag{8}$$

where A is a constant that has to be determined by experiment. Dryden and Simmons and Salter, whose experimental results are reviewed by Taylor, found $1.95 \leq A \leq 2.20$ for a large variety of different grids. The best fit to the present results was obtained with $A_1 = 1.976$ (screen 1) and $A_2 = 2.028$ (screen 2). Departures from the linear law that occur for small x/M are due to the "shadow" of the grid (see the "Experimental Setup" section). For large x/M, the influence of the natural, nongrid-induced turbulence becomes apparent. For $(x/M) \to \infty$, both curves have to fit the dashed line in Fig. 4, which indicates the wind-tunnel turbulence intensity without any screens.

Figure 5 shows the macroscale of turbulence vs distance from the screen. As can be seen, the data for both grids fall on a single straight line, at least for the initial period of turbulence decay until about $(x/M) = 60$–70.

Figure 6 gives the values of the Taylor microscale (dissipative scale). Though more data would be desirable, it seems that λ/M also increases linearly with x/M.

Experimental data about the increase of U_∞/u', L/M, and λ/M with x/M, which is available in the literature, often look somewhat confusing. According to Taylor,[5] Eqs. (2) and (8) hold for isotropic turbulence. This means that $(U_\infty/u') \sim (x/M)$ and $(\lambda/M) \sim (x/M)^{1/2}$. The macroscale in Taylor's analysis (M) is invariant to changes of x/M (isotropy!).

According to Corrsin,[12] the stationary but streamwise inhomogeneous turbulence behind a periodic grid at large Reynolds numbers is a useful approximation to isotropic turbulence ("nearly isotropic turbulence"). For this type of flow, Corrsin suggests

$$\frac{\lambda}{L} = B\sqrt{\frac{\nu}{L \cdot u'}} \tag{9}$$

as a relation between dissipative scales and macroscales. Equation (9) is identical with Taylor's Eq. (2), except for a different constant (B) and M being replaced by its nonconstant counterpart L (macroscale) for streamwise inhomogeneous turbulence. For the present experimental results, $(U_\infty/u') \sim (x/M)$ and $(L/M) \sim (x/M)$, Eq. (9) predicts $(\lambda/M) \sim (x/M)$, which is in agreement with the measurements displayed in Fig. 6. Thus the present experimental setup provides grid-induced turbulence, which is consistent with the laws of "nearly isotropic turbulence." However, this is restricted to the region between 30 and 60 mesh lengths behind the screen. At shorter distances, the influence of the individual wakes becomes apparent and for $(x/M) > 60$ U_∞/u' and L/M depart from the linear increase with x/M. In the case of U_∞/u', this is due to large-scale turbulence, which is in the airstream before striking the grid. Apparently, the grid does not remove this turbulence completely.

In Figs. 7–9 pressure distributions in the model's plane of symmetry are shown. Figure 7 shows data for the flow without screens at different Reynolds numbers with the model positioned at $x = 1.2$ m behind the nozzle. There is a strong dependence of the pressure coefficient c_p on the Reynolds number, at least at the positions 1 and 7, where there are the critical radii R_1 and R_7 in the notation of Fig. 2.

The streamlines along the hood were visualized with the help of the oil film technique. It was found that a big recirculation region extended from R_1 down to the windscreen, position 2, for $Re < 3.3 \times 10^6$.

Figure 8 shows the pressure distribution for the same range of Reynolds numbers but with screen 1 in the nozzle exit. The

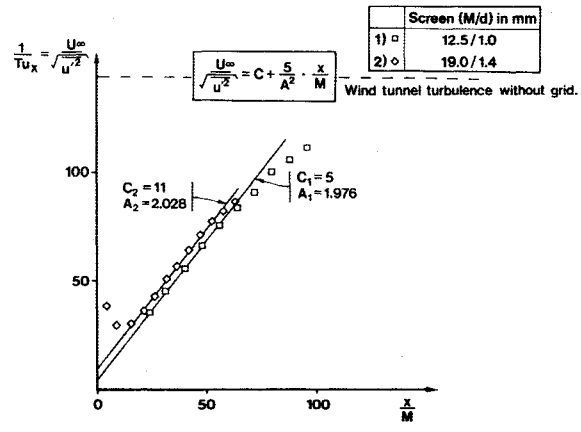

Fig. 4 Inverse turbulence intensity behind screens. Comparison with Taylor's theory.[5]

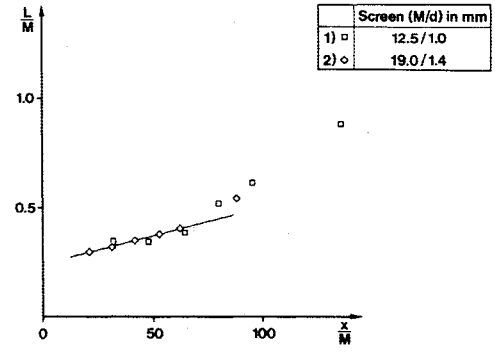

Fig. 5 Macroscale of turbulence behind screens.

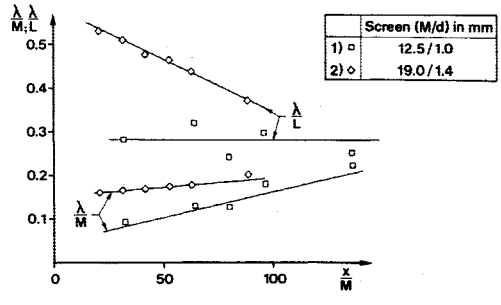

Fig. 6 Taylor microscale of turbulence behind screens.

model leading edge was positioned at $x = 0.6$ m behind the screen ($-48M_1$). As a reference, one curve without a screen taken from the previous figure is presented as well: model 1:2.5, $Re = 5.2 \times 10^6$.

As can be seen, the results nearly fall on a single line. Only at position 7 is there still a significant Re effect. A comparison with the reference curve shows good conformity with the pressure distribution for $Re = 2.7 \times 10^6$ (scale 1:2.5) with screen 1 in use, indicating an increase of the "effective Reynolds number" by a factor of $(5.2/2.7) = 1.93$. The same plot is shown in Fig. 9 for screen 2. The model position was also $x = 0.6$ m ($-32M_2$).

The shift in the effective Reynolds number seens to be even more pronounced than in the previous figure, as can be concluded from the weaker Re dependence at positions 1 and 7. As a reference, the c_p distribution for $Re = 5.2 \times 10^6$ without screen is used in Fig. 9 once again. Just like in the previous figure, for several of the smaller Reynolds numbers in conjunction with screen 2, the suction peak at position 7 reaches even higher values than for the reference curve. In this case, the reference can be matched best for $Re = 2.0 \times 10^6$ (scale

1:4). As this result originates from a physically different model, it might be subject to manufacturing accuracy. Therefore, it is preferred to look exclusively for the pressure distribution of the 1:2.5 scale model that matches the reference curve best. This is the case for $Re = 2.7 \times 10^6$. Thus, the effective Reynolds number is increased by a factor of 1.93 once again. Strictly, the increase is even bigger because $Re = 2.7 \times 10^6$ already leads to a stronger suction peak at position 7 than does the reference curve. This is substantiated by a comparison of the turbulence decay curves in Fig. 4. At $x = 0.6$ m, one finds $Tu_x = 1.5\%$ for screen 1 ($x/M_1 = 48$) and 2.0% for screen 2 ($x/M_2 = 32$).

Figures 10 and 11 show the effect of the model location on the pressure distribution behind screens 1 and 2, respectively. The Re number is constant, $Re = 2.1 \times 10^6$, i.e., in a range where c_p is strongly dependent on Re. Both figures include the same reference curve: the highest possible Re number ($Re = 4.6 \times 10^6$) in combination with screen 2 at $(x/M_2) = 32$ (see also Fig. 9). This c_p distribution can be expected to provide us with the highest effective Reynolds number in this study.

As the grid-induced turbulence intensity decreases with increasing distance from the grid (see Fig. 4) and the turbulent macroscale increases at the same time (see Fig. 5), the effectiveness of the screen should diminish rapidly when the model is positioned far behind the screen. In Fig. 10, one can observe a considerable dependence of the pressure distribution, not only at the model radii 1 and 7, but on x/M_1, provided the distance from the screen is greater or equal to $x = 1.0$ m ($-80M_1$). In the case of screen 2 (Fig. 11), the same thing happens at $x = 1.2$ m ($-63M_2$). Of course, more data would be necessary to locate precisely the model-to-screen distance $(x/M)_{max}$ that should not be exceeded in order to measure pressure data that does not depend on the actual x/M. However, a cross check with Fig. 4 indicates that for $(x/M_1) = 80$ and $(x/M_2) = 63$, the values of Tu_x lie closely together. They are 1.0% at $(x/M_1) = 80$ behind screen 1 and 1.1% at $(x/M_2) = 63$, behind screen 2.

This leads to the conclusion that for $Re = \text{const}$ different screens may produce the same flow pattern at the model. Of course, this leads to identical pressure distributions for different physical locations of the model in relation to the screen, as long as the turbulence intensity and structure is equal at these positions. This is consistent with Taylor's theory [Eq. (6)] and Dryden's measurements (Fig. 1) for the flow around a sphere.

Figure 12 shows the drag coefficient of the vehicle vs Re number with and without turbulence manipulation. The model location is constant, i.e., $x = 0.6$ m behind the screen and the nozzle. Without a screen ("clean flow"), there is a steady decrease of c_D up to the highest Re that could be realized ($Re = 5.2 \times 10^6$). Both screens 1 and 2 lead to a considerable decrease of drag, especially at small Reynolds numbers. Whereas the clean flow needs about $Re = 3.8 \times 10^6$ to yield $c_D = 0.30$ (model 1:2.5), using screen 1 or 2, this can already be achieved at $Re = 2.5 \times 10^6$ and—with extrapolation of the available data for screen 2—$Re = 2.2 \times 10^6$, respectively. This is equivalent to an increase of the effective Reynolds number by a factor of (3.8/2.5) = 1.52 for screen 1 and (3.8/2.2) = 1.73 for screen 2. These factors are considerably smaller than those deduced from the pressure distribution (previously discussed). The explanation for that could be as follows.

In contrast to c_p, the drag coefficient is dependent not only on the transition and separation behavior of the flow but also on the effect of wall shear stress. Thus, the asymptotic value of c_D for large Reynolds numbers might be higher for the flow behind a screen than for the clean flow, because additional turbulence can intensify the Reynolds stresses in the boundary layer.[7-11] So, due to the influence of the nonconstant wall shear stresses, comparing effective Reynolds numbers for constant values of c_D necessarily leads to errors because the result depends on the c_D value under consideration and its specific wall shear component, as can be verified easily from Fig. 12.

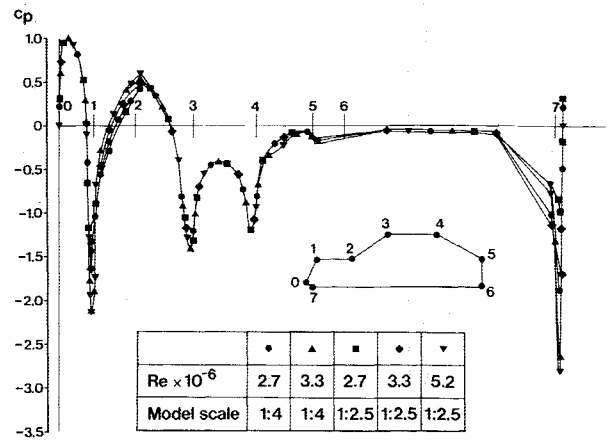

Fig. 7 Pressure distributions on a road vehicle at different Reynolds numbers.

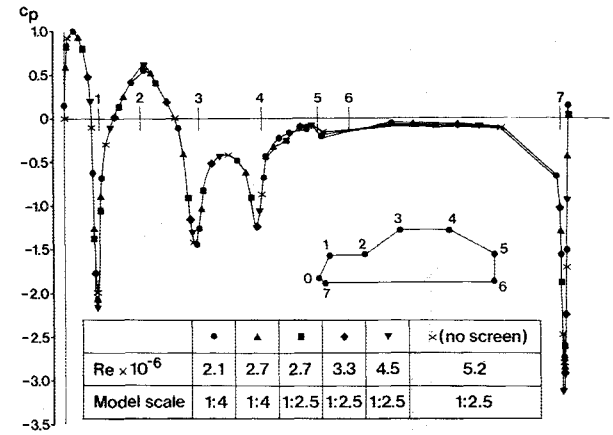

Fig. 8 Pressure distributions on a road vehicle at different Reynolds numbers. Turbulence modified by screen 1.

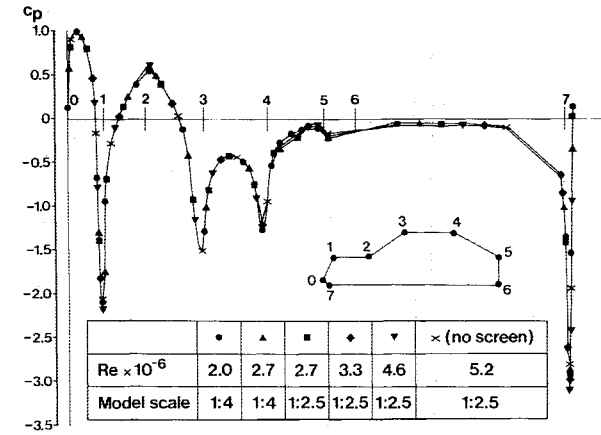

Fig. 9 Pressure distributions on a road vehicle at different Reynolds numbers. Turbulence modified by screen 2.

Unfortunately, the drag curve of Fig. 12 has no distinguished points like minima or maxima. Otherwise, the Re values of those points could be used as a measure for the increase of the effective Reynolds number. This procedure, however, would avoid the aforementioned problems.

As already discussed for c_p, there is also a dependence of c_D on the scale of the model under investigation for $Re = \text{const}$ (see Fig. 12). It seems unlikely that this is entirely due to the accuracy of manufacturing. It could as well be an interference effect between the sting and the model or between the wake of the model and the collector at the end of the test section. The latter is qualitatively consistent with the findings of von

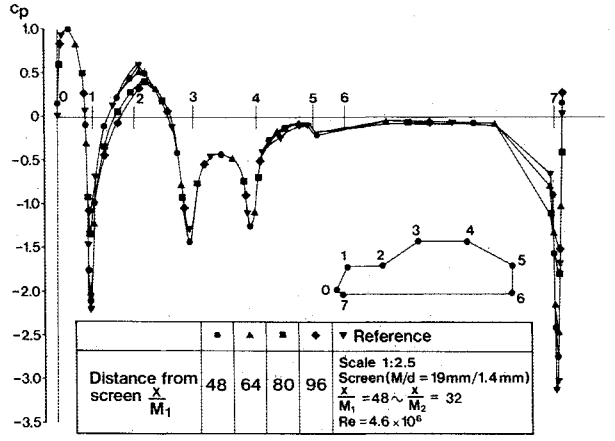

Fig. 10 Effect of the model position behind screen 1 on the pressure distribution for $Re = 2.1 \times 10^6$.

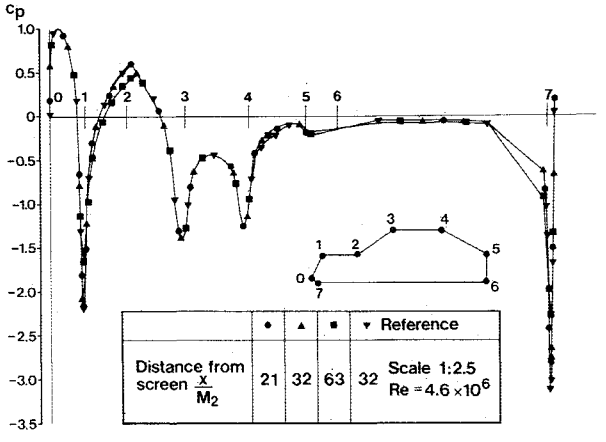

Fig. 11 Effect of the model position behind screen 2 on the pressure distribution for $Re = 2.1 \times 10^6$.

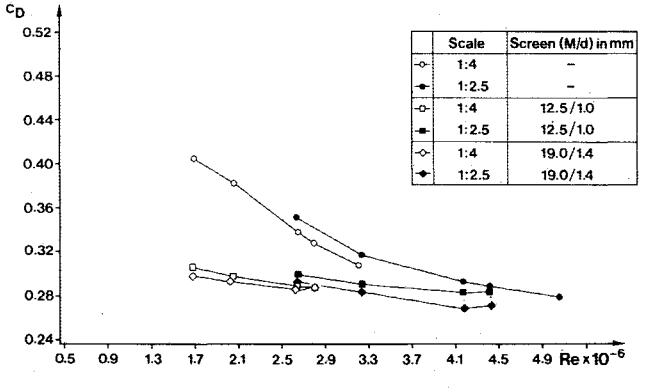

Fig. 12 Drag coefficient of a road vehicle without ground plane vs Reynolds number.

Schulz-Hausmann and Vagt,[13] who showed that conventional design of open-jet test sections leads to a loss in base pressure of bluff bodies the wakes of which extend downstream into the collector. Their study, however, basically dealt with stronger wake and collector interactions than those that can be expected in the present case. Nevertheless, for industrial purposes, i. e., for developing and optimizing the shape of a new vehicle, a result like the one shown in Fig. 12 is of great help. For the present experimental conditions, it tells the engineer

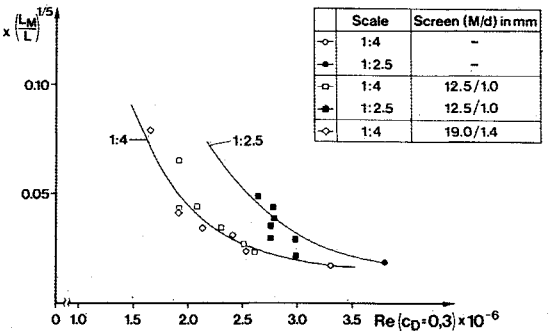

Fig. 13 Taylor's turbulence parameter (intensity times 1/5th power of scale) for a road vehicle.

that whether or not the absolute c_D level is correct, he can be sure of simulating full-scale Re numbers at about $Re = 4.1 \times 10^6$.

Figure 13 shows the results of the drag measurements plotted in Taylor's coordinates [see Eq. (6)], except for M again being replaced by the actual macroscale L at the model location ("nearly isotropic turbulence"). This is analogous to the plot published by Dryden for the flow around a sphere (see Fig. 1). As it was not possible to define a critical Reynolds number for the vehicle shape, the abscissa is formed with $Re(c_D = 0.30)$.

All the data for each of the two models fall reasonably well on a single line. As there are c_D differences between the two models for Re = const (see previous discussion), Fig. 13 reveals two functions $F(Re)$. The data that do not match any of the two curves are due to 1) model positions close to the grid where the individual wakes of the rods are not perfectly mixed and 2) horizontal buoyancy: higher values of Re and $Tu_x(L_M/L)^{1/5}$ are required in order to meed $c_D = 0.30$. In general, however, Taylor's analysis about turbulence manipulation by screens obviously holds for the case of a vehicle shape.

Figure 13 is well suited to come back to the question of effective Reynolds numbers. Each point on the curves provides $Re(c_D = 0.30)$ and $Tu_x(L_M/L)^{1/5}$ for $Re_{\text{eff}} = Re(c_D = 0.30$, no screen$) = 3.3 \times 10^6$ (model 1:4) and 3.8×10^6 (model 1:2.5). As the data for the quarter-scale model covers the interval $1.66 \times 10^6 < Re < 3.3 \times 10^6$, the ratio of effective to real Reynolds number lies between 1.99 and 1. For the 1:2.5 model, the interval is $2.6 \times 10^6 < Re < 3.8 \times 10^6$, leading to a ratio between 1.46 and 1. If more effective screens were available, the curves of Fig. 13 could be continued to the lower Re range, which would be equivalent to a higher relative increase in the effective Reynolds number.

Summary

From the "Statistical Theory of Turbulence" by Taylor,[4,5] it is known that the Reynolds number corresponding to the location x_{tr} of transition is a function of $Tu(x_{tr}/M)^{1/5}$, i.e., a parameter consisting of intensity and scale of isotropic turbulence. For the case of a sphere, a constant location of transition leads to a constant location of the separation point and thus to an almost constant value of the pressure drag, which makes up the major component of the total drag. So, a "critical" Reynolds number (Re_{crit}) can be defined that provides a certain drag coefficient (e.g., $c_D = 0.3$). According to Taylor, Re_{crit} is a function of $Tu(D/M)^{1/5}$ [see Eq. (6)]. In general, these considerations were verified by Dryden's experimental work.[6]

In the present paper, Taylor's considerations are applied to road vehicle aerodynamics. The goal of the work was to find out whether the Re number associated with a certain value of c_D behaves in an analogous way to the case of the sphere. This can be expected if the vehicle drag is mainly made up by pressure drag and if the shape gives rise to a dependency between the locations of transition and separation.

Thus, two principle models of a road vehicle differing only by their scales (1:4 and 1:2.5) were designed and tested in the wind tunnel of the Technical University of Darmstadt. The tests were performed without a ground plane to separate freestream turbulence effects on the models from possible effects on the boundary layer on the ground board. From the literature[7-11] it is known that there is an increase in boundary-layer thickness and a decrease in displacement and momentum thickness for the turbulent boundary layer on a flat plate in a turbulent freestream. In principle, this has to be considered when investigating the flow around a road vehicle. The basic physical effects due to freestream turbulence, however, which were observed in this study, still remain valid.

As foreseen, there was a large separation bubble on the hood for Re numbers below 3.3×10^6. Flow visualization showed that the extension of separation was reduced with increasing Reynolds number, while c_D was decreased and the suction peaks at the front radii became more pronounced.

The same flow changes that occurred when increasing the Reynolds number also could be achieved by appropriate turbulence manipulation immediately at the end of the nozzle for considerably smaller Reynolds numbers. Two alternative turbulence grids with mesh sizes of $M_1 = 12.5$ mm and $M_2 = 19$ mm and bar diameters of $d_1 = 1$ mm and $d_2 = 1.4$ mm were used. The screens produced turbulence intensities between 2.2 and 2.8% at the closest model location ($x = 0.4$ m behind the screen) and 0.8 and 1%, respectively, at the furthest backward position ($x = 1.7$ m).

Due to problems with horizontal buoyancy and possible interactions of the model wake and the collector of the open-jet test section, there was an influence of the model scale on the pressure and drag results. Therefore, if plotted in coordinates analogous to those used by Taylor,[4] only the results from each scale almost match a single line (see Fig. 13). Nevertheless, the potential of turbulence manipulation as a means of simulating full-scale Reynolds number flow on small-scale vehicle models could be demonstrated. With the screens under investigation, a maximum increase of the effective Reynolds number by a factor of about two was achieved. Higher increases just require more powerful turbulence manipulation.

References

[1]Wiedemann, J. "Theoretical and Experimental Optimization of the Road-Vehicle Internal Flow," *von Kármán Institute For Fluid Dynamics Lecture Series 1986-05 on Vehicle Aerodynamics,* Rhode-St.-Genese, Belgium, March 1986.

[2]Wiedemann, J., "Grenzen and Möglichkeiten der Modelltechnik innerhalb der Kraftfahrzeug-Aerodynamik," *Aerodynamik des Kraftfahrzeugs,* Haus der Technik, Essen, FRG, Symposium T-30-905-056-7, 1987.

[3]Soja, H. and Wiedemann, J., "The Interference Between Exterior and Interior Flow on Road Vehicles," *Societe des ingenieurs de l'automobile (S.I.A.), Journees d'etude: Dynamique du vehicule—securite active,* June 16-17, 1987.

[4]Taylor, G. I., "Statistical Theory of Turbulence. Part V," *Proceedings of the Royal Society of London,* Series A, Mathematical and Physical Sciences, London, 1936, pp. 307-317.

[5]Taylor, G. I., "Statistical Theory of Turbulence. Part I-IV," *Proceedings of the Royal Society of London.* Series A, Vol. 151, 1935, pp. 421-478.

[6]Dryden, H. L., Schubauer, G. B., Mock, W. C., Jr., and Skramstad, H. K., "Measurements of Intensity and Scale of Wind-Tunnel Turbulence and Their Relation to the Critical Reynolds Number of Spheres," NACA Rept. 581, 1936.

[7]Meier, H. U., "The Response of Turbulent Boundary Layers to Small Turbulence Levels in the External Free Stream," International Conf. of Aeronautical Sciences, ICAS Paper 76-05, 1976.

[8]Meier, H. U. and Kreplin, H. P., "Influence of Freestream Turbulence on Boundary Layer Development," *AIAA Journal,* Vol. 18, Jan. 1980, pp. 11-15.

[9]Bradshaw, P., "Effect of Free Stream Turbulence on Turbulent Shear Layers," Imperial College, London, Aero Rept. 74-10, 1974.

[10]Hancock, P. E., "The Effect of Free Stream Turbulence on Turbulent Boundary Layers," Ph.D. Thesis, Imperial College, London, 1980.

[11]Hancock, P. E. and Bradshaw, P., "The Effect of Free Stream Turbulence on Turbulent Boundary Layers," *Journal of Fluids Engineering,* Vol. 105, No. 3, Sept. 1983, pp. 284-289.

[12]Corrsin, S., "Experimental Methods," *Handbuch der Physik.* Vol. VIII/2, edited by S. Flügge and C. Truesdell, Springer-Verlag, Berlin, 1963, pp. 524-590.

[13]von Schulz-Hausmann, F. K. and Vagt, J. D., "Influence of Test-Section Length and Collector Area on Measurements in 3/4-Open-Jet Automotive Wind Tunnels," Society of Automotive Engineers, Warrendale, PA, Paper 880251, 1988.